JOURNAL OF Applied Polymer SCIENCE

Correlation between the fracture toughness and β-crystal fraction in a β-nucleated propylene-based propylene–ethylene random copolymer

Chunbo Zhang, Guoming Liu, Qianhong Jiang, Ying Zhao, Dujin Wang

Beijing National Laboratory for Molecular Sciences, Key Laboratory of Engineering Plastics, Institute of Chemistry, Chinese Academy of Sciences, Beijing 100190, China

Correspondence to: G. Liu (E-mail: gmliu@iccas.ac.cn) and Y. Zhao (E-mail: yzhao@iccas.ac.cn)

ABSTRACT: Propylene-based propylene–ethylene random copolymer (PPR) has been widely used in the production of hot-water pipes. To further improve its toughness and thermal resistance, β-nucleating agents (β-NAs) are frequently incorporated. In this study, PPR containing 5.6 mol % ethylene units was modified by two kinds of β-NAs, that is, calcium pimelate and *N,N′*-dicyclohexylterephthalamide. The notched Izod impact strength of PPR increased with the addition of the β-NAs. Drastically different toughening effects were found between the two β-NAs. The structure of PPR with and without a β-NA was investigated by calorimetry, X-ray diffraction, and thermomechanical analysis. The results indicated that the relative fraction of β crystals (k_β) in the injection-molded specimens was determined by the type and content of β-NA. The relationship between k_β and the impact toughness was summarized. A critical value for k_β (0.68) was identified for the brittle–ductile transition of PPR. PPR with β-NA having a k_β greater than 0.68 displayed a higher impact strength than the other mixtures. © 2015 Wiley Periodicals, Inc. J. Appl. Polym. Sci. **2016**, *133*, 42930.

KEYWORDS: crystallization; mechanical properties; polyolefins; properties and characterization

Received 30 June 2015; accepted 9 September 2015

DOI: 10.1002/app.42930

INTRODUCTION

The random copolymerization of propylene with other α-olefins has been proven to be an effective method for broadening the application of isotactic polypropylene (iPP). For instance, iPP has relatively poor impact resistance, and its toughening modification has received scientific and industrial attention for decades.[1–4] When copolymerizing with a certain amount of ethylene units, propylene–ethylene random copolymers (PPR) were found to be more ductile and tougher than iPP.[5] The toughness of PPR can be further enhanced by the addition of β-nucleating agents (β-NAs).[6–8] As an important way to improve the fracture toughness of iPP, the structure and properties of β crystals have been studied extensively.[1,9–13] The bundled lamellar arrangement in β spherulites,[14–16] stress-induced crystal transition,[9,10] and formation of voids[16,17] are considered to be relevant to the toughness enhancement. The loose lamellar packing allows the easier initiation and propagation of plastic deformation under impact. The crystal transition and cavitation of β crystals during tensile deformation have been confirmed by many researchers.[18–20] All of these factors favor the energy dissipation process of iPP with a high β-crystal content. At this point, the intrinsic mechanism of the high toughness of iPP crystallized predominately in β crystals is still not fully understood.

The fracture toughness of iPP is affected by the β-crystal content, and this is determined by the type of β-NA, the content of β-NA,[11,21] and the thermal treatment.[6,22–24] Most β-NAs, such as γ-modified linear *trans*-quinacridone, calcium salts of suberic or pimelic acid, and aryl amide compounds, can efficiently induce the formation of β crystals in iPP, and the relative fraction of β crystals (k_β) generally exceeds 60%.[13,21,24–27] However, the introduction of ethylene comonomers in PPR greatly decreases the tendency to form β crystals. In particular, for those β-NAs with dual nucleating effects for α and β crystals, k_β in PPR hardly reaches 50%.[6,28] Calcium pimelate (Ca-Pim), on the other hand, exhibits high nucleating efficiencies for both iPP and PPR. The β-crystal content in PPR can reach 90% through the addition of Ca-Pim.[29]

A number of reports have covered the influence of the β-NA content on the mechanical properties of iPP and PPR.[6,30–34] However, the quantitative correlation between the mechanical properties and β-crystal content of PPR has not been established. In this study, k_β in β-nucleated PPR was tuned in a broad range by the type and content of β-NA which made it possible for us to investigate the relationship between the β-crystal content and the mechanical properties of PPR. The brittle–ductile transition of PPR as a function of the β-crystal content was revealed. This study may provide a reference for the β modification of polypropylene to achieve high performance.

EXPERIMENTAL

Materials

PPR prepared by a Ziegler–Natta catalyst was obtained from SINOPEC Beijing Yanshan Co. The melt flow rate of PPR was 1.8 g/10 min; this was measured under a load of 2.16 kg at 230°C. The weight-average molecular weight was 5.77×10^5 g/mol, and the polydispersity index was 3.54. The fraction of ethylene was about 5.6 mol %, as determined by ^{13}C-NMR. Ca-Pim, a selective β-NA, was synthesized by the neutralization reaction of $Ca(OH)_2$ (Xilong Chemical Co., Ltd.) and pimelic acid (Sigma-Aldrich). *N,N′*-Dicyclohexylterephthalamide (trade name TMB-5) was supplied by Shanxi Chemical Research Institute Co., Ltd. According to previous works,[26,35] TMB-5 has dual-nucleating ability to enhance the crystallization of α and β crystals depending on the crystallization conditions. An antioxidant, Irganox B215 (Ciba-Geigy) composed of 2:1 Irgafos 168/Irganox 1010 was used to prevent thermooxidative degradation during processing.

Sample Preparation

A two-step mixing process was applied to prepare PPR samples with different weight fractions of β-NA. The Ca-Pim or TMB-5 powders were first melt-blended with PPR to obtain a masterbatch containing 2 wt % β-NA. Then, the masterbatch was melt-mixed with pure PPR to dilute the contents of β-NA to 0.025, 0.05, 0.1, 0.25, and 0.5 wt %. At each mixing step, 0.1 wt % antioxidant was added to the samples. A pure PPR sample was also prepared with the same processing history for comparison. Melt blending was carried out in a twin-screw extruder (Thermo Scientific Haake RheomixOS) at a screw rotation speed of 150 rpm. The processing temperature was within 215–220°C. The pelletized samples were then injection-molded into specimens for mechanical tests in accordance with ISO standards. Rectangular and dumbbell-shaped samples were used for impact/flexural measurements and tensile testing, respectively. Injection molding was conducted on a machine (UN120A, Guangdong, Yizumi Seiki Machinery Co., Ltd., China) at melt temperatures within 190–215°C. The injection pressure was 38 bar, and the mold temperature was room temperature. The specimens were kept at room temperature for more than 1 month before measurements.

Mechanical Measurements

The notched Izod impact strength of specimens was measured with an Izod impact machine (XJC-250) according to ISO 179-1982. The tensile and three-point flexural measurements were carried out with an Instron 3365 universal tensile testing machine according to ISO 527-1BA and ISO 178-1993, respectively. The crosshead speeds for the tensile and flexural measurements were 50 and 2 mm/min, respectively. All of the mechanical measurements were carried out at room temperature. The average values shown in the results were obtained from at least five specimens.

Differential Scanning Calorimetry (DSC)

The calorimetric analysis of the samples was conducted with a TA Instruments DSC Q2000. The instrument was calibrated with indium before the measurements. The samples cut from the skin and core layers of the specimens were heated at 10°C/min from 40 to 200°C under the protection of nitrogen atmosphere.

Wide-Angle X-ray Diffraction (WAXD)

WAXD was used to characterize the multilayer structures in the injection-molded bars. Skin and core layers were cut from the middle of the injection-molded specimens along the flow direction, and the thickness of each layer was less than 100 μm. WAXD measurements were carried out at beamline BL16B1 ($\lambda = 1.24$ Å) at the Shanghai Synchrotron Radiation Facility. The scattering patterns were captured by a MAR charge coupled device (MAR–USA) detector with a resolution of 2048×2048 pixels (pixel size = 79 μm). The pattern acquisition time was 30 s, and the sample-to-detector distance was 181 mm. Air scattering was subtracted from the experimental data before further analysis.

Dynamic Mechanical Analysis (DMA)

DMA tests were carried out with a DMA Q800 analyzer (TA Instruments). Rectangular samples with dimensions of $30 \times 10 \times 4$ mm^3 (Length × Width × Thickness) were measured in single-cantilever mode. The samples were heated from −100 to 120°C at 3°C/min and at an oscillatory frequency of 1 Hz. The strain was set to be 0.05%.

Scanning Electron Microscopy (SEM)

The morphologies of the fracture surfaces of the PPR specimens prepared by a notched Izod impact test at room temperature were observed on a JEOL JSM 6700 scanning electron microscope operated at an accelerating voltage of 5 kV. The samples were platinum-sputtered before SEM observation.

RESULTS AND DISCUSSION

Mechanical Properties of PPR with Different β-NA Contents

The impact strength of PPRs with different kinds and contents of β-NAs is shown in Figure 1(a). In the absence of a β-NA, PPR exhibited a relatively low notched Izod impact strength (5.4 kJ/m^2). As the β-NA content increased, the notched Izod impact strength increased. The impact strength reached a maximum at a low nucleating agent (NA) load. When the β-NA content was increased further, the impact strength decreased slowly. The variation trend of the impact strength as a function of the β-NA content was similar to that in iPP/β-NA systems.[11,30,36] Obviously, the two β-NAs were different in toughening PPR. The maximum impact strength obtained by the addition of Ca-Pim was more than three times that obtained by TMB-5. On the other hand, as shown in Figure 1(b), the yield strength of PPR was almost not affected by the introduction of β-NAs. The flexural modulus of PPR increased slightly with the addition of TMB-5, whereas it was influenced less by Ca-Pim. The previous results indicated that the β crystals improved the toughness of PPR without obvious sacrifices of other mechanical properties. The different mechanical responses of PPR with and without a β-NA were considered to be related to the structure; this is discussed in more detail later.

Melting Behavior

As is well known, the injection-molded bar usually displays a multilayer structure that results from the different cooling conditions and the stress field during solidification. Three layers, including the skin, subskin, and core layer, have been identified

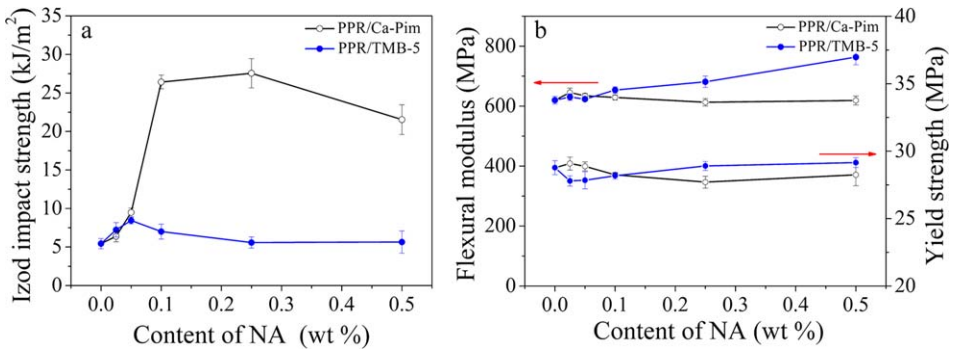

Figure 1. Mechanical properties of PPR with Ca-Pim and TMB-5 as a function of the β-NA content: (a) notched Izod impact strength and (b) flexural modulus and yield strength. The tests were performed at room temperature. [Color figure can be viewed in the online issue, which is available at wileyonlinelibrary.com.]

in injection-molded iPP samples.[32,37,38] In this study, the crystalline structure of the skin and core layers in the PPR samples were characterized by DSC and WAXD, respectively. The DSC heating curves are shown in Figure 2. Only one endothermic peak located at 140°C, corresponding to the melting of α crystals, was observed in the PPR without a β-NA. Another melting peak at about 125°C, originating from β crystals, emerged in the DSC heating curves of the PPR with a β-NA. The melting peak of β crystals in the core layer [Figure 2(a,c)] was more obvious than that in the skin layer [Figure 2(b,d)]. The area of the β-crystal melting peak in the core layer of PPR/Ca-Pim was larger than that of the PPR/TMB-5 samples, and the area was influenced by the β-NA content. As shown in Figure 2(a), PPR with 0.05 wt %TMB-5 displayed a larger β-crystal melting peak than other PPR/TMB-5 samples. This was consistent with the impact strength results shown in Figure 1(a). Similarly, the specimen with 0.25 wt % Ca-Pim showed the best impact strength and had the largest β-crystal melting peak in the core layer [Figure 2(c)].

The melting peaks of the α crystals were asymmetric; this indicated that the lamellar thickness in the α crystals had a wide distribution. Another reason for the asymmetric α melting peak for the PPR/β-NA samples may have been the formation of α crystals via recrystallization from melted β crystals during heating.[29] It was found that there was a critical temperature of

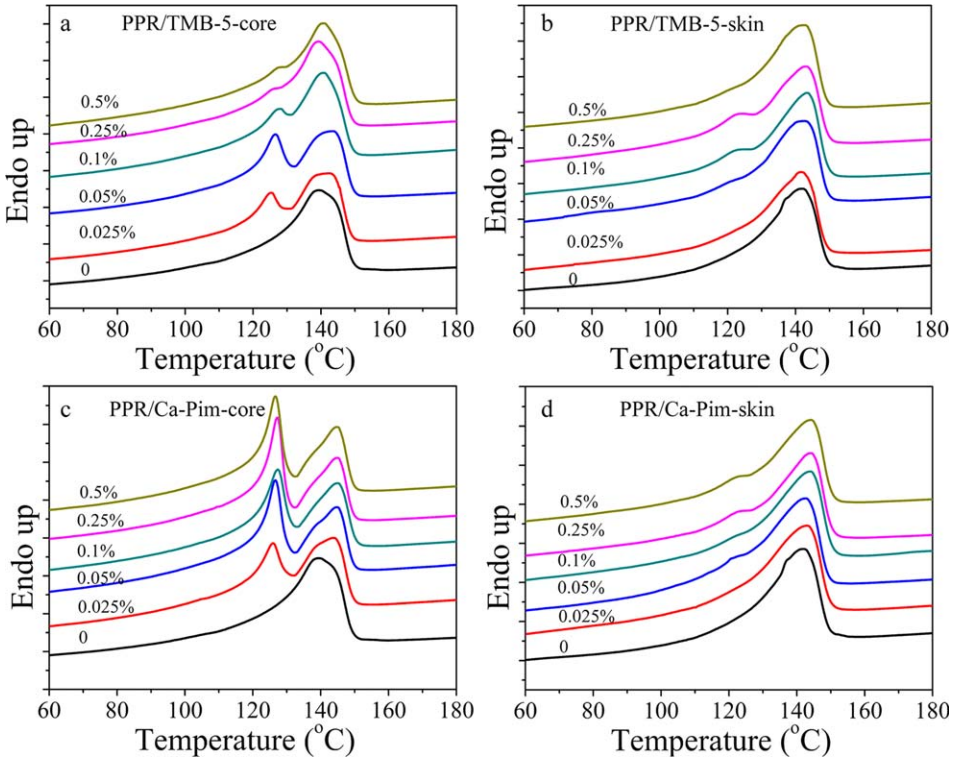

Figure 2. DSC heating curves of PPR with different β-NAs: (a) core layer in PPR/TMB-5, (b) skin layer in PPR/TMB-5, (c) core layer in PPR/Ca-Pim, and (d) skin layer in PPR/Ca-Pim. The β-NA content is shown in the graphs. The heating rate was 10°C/min. [Color figure can be viewed in the online issue, which is available at wileyonlinelibrary.com.]

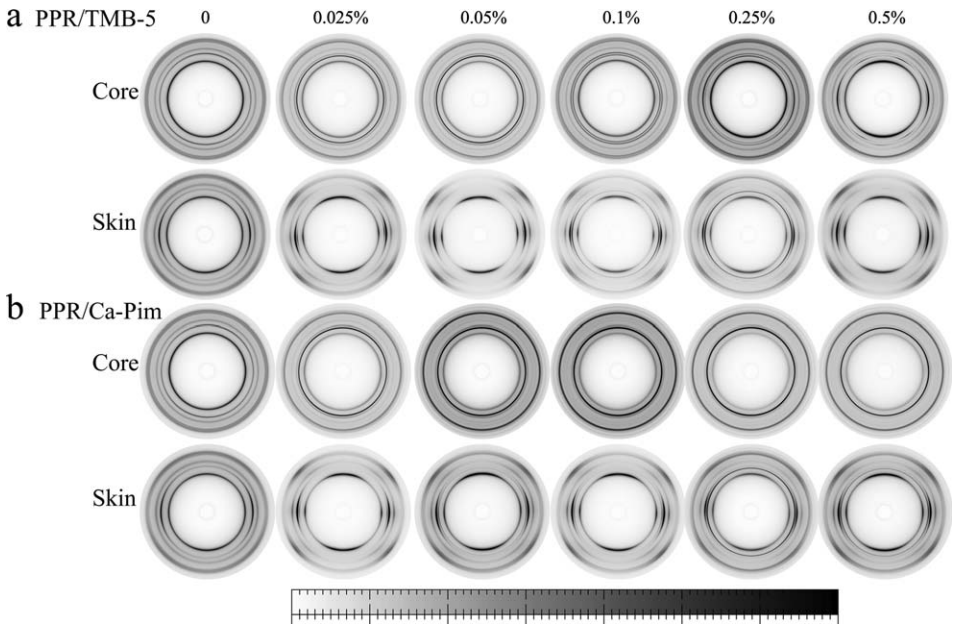

Figure 3. 2D WAXD patterns of PPR with different β-NAs: (a) PPR/TMB-5 and (b) PPR/Ca-Pim. The β-NA content and the sampling location are shown in the graphs.

cooling ($T_R^* \approx 100°C$) in a β-modified polypropylene system, below which the recrystallization from β crystals to α crystals happened during the subsequent heating process.[22] The recrystallization in our samples could not be eliminated because the cooling temperature was lower than T_R^*. Consequently, the quantitative analysis on the β-crystal content in the PPR/β-NA samples could not be obtained from the calorimetric measurement.

Effects of the β-NAs on the Crystalline Orientation Behavior

The two-dimensional (2D) WAXD patterns of the core and skin layers in the PPR samples are presented in Figure 3. The orientation of the α and β crystals in the core layer was not obvious. The degree of crystalline orientation in the skin layer was obviously higher than that in the core layer because of the strong shear stress that the skin layer experienced.[32] The obvious orientation of the core layer in PPR/0.5 wt % TMB-5 was observed. This may have resulted from the orientation of rodlike TMB-5 in the PPR matrix during flow; thereby, oriented β crystallites were induced through epitaxial crystallization.[39,40] To further describe the orientation of crystallites in the skin layer, the full width at half-maximum (FWHM) of the 110_α and 110_β peaks was calculated from azimuthal intensity profiles. Generally, a lower value of FWHM is associated with a more oriented structure,[41] so the 1/FWHM value shares the same trend with the degree of crystalline orientation. In Figure 4(a), the orientation of α crystals showed an increase when a small amount of β-NA was added and a slight decrease when the β-NA content was increased further. The increase in the β-NA content significantly suppressed the orientation of β crystals induced by shear stress, as presented in Figure 4(b). The orientation of β crystals in PPR/TMB-5 was higher than that in PPR/Ca-Pim; this may have been due to the anisotropic morphology of TMB-5.[42] The crystalline orientation in the skin layer is thought to be beneficial for the tensile and impact strength of a material.[38] Many other factors also influenced the mechanical properties, and therefore, a qualitative relationship was not observed between the results shown in Figures 1 and 4.

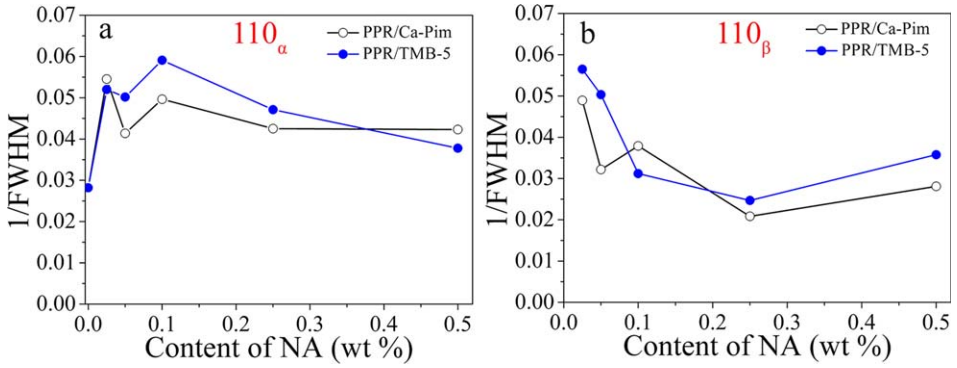

Figure 4. 1/FWHM obtained from the azimuthal intensity profiles on the equator of (a) 110_α and (b) 110_β in the skin layer as a function of the β-NA content. [Color figure can be viewed in the online issue, which is available at wileyonlinelibrary.com.]

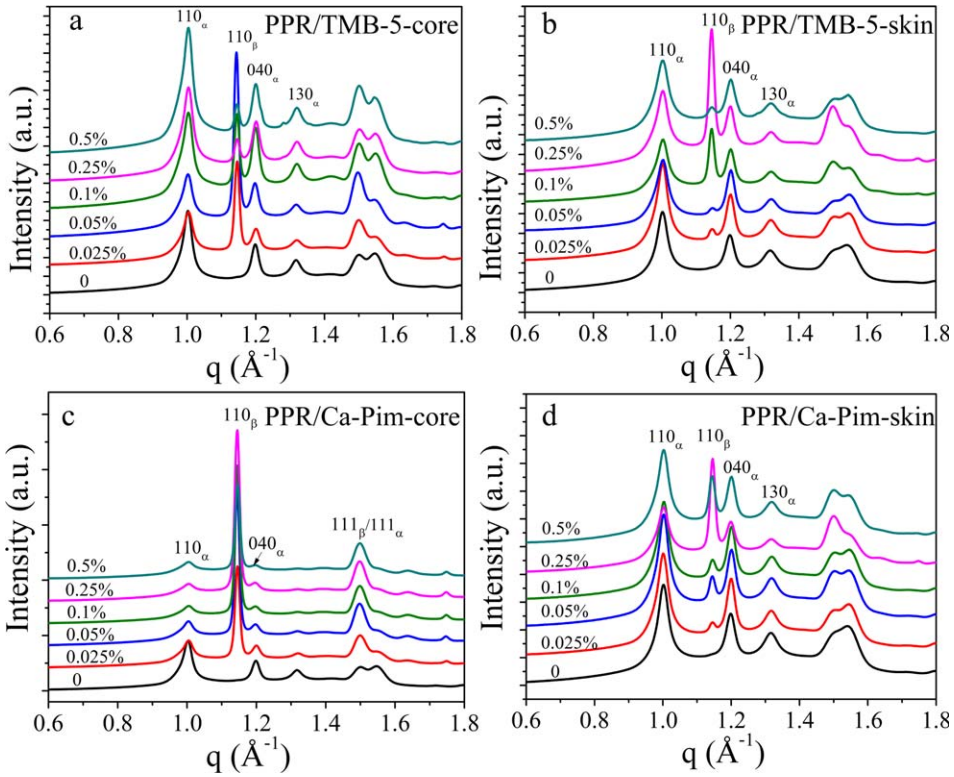

Figure 5. 1D WAXD profiles of PPR with different β-NAs obtained from circularly integrated intensities of 2D WAXD patterns: (a) core layer in PPR/TMB-5, (b) skin layer in PPR/TMB-5, (c) core layer in PPR/Ca-Pim, and (d) skin layer in PPR/Ca-Pim. The scattering vector ($\mathbf{q}$) is defined as $\mathbf{q} = 4\pi \times \sin\theta/\lambda$, where 2θ is the Bragg angle and λ is the wavelength of radiation. The β-NA content is shown in the graphs. [Color figure can be viewed in the online issue, which is available at wileyonlinelibrary.com.]

Crystallinity Index (X_c)

Figure 5 displays the one-dimensional (1D) WAXD profiles of the PPR samples obtained from the circularly integrated intensities of the 2D WAXD patterns in Figure 3. The pure PPR contained only α crystals; nevertheless, the PPR samples with β-NAs had both α and β crystals. The intensity of 110_β in the skin layer [Figure 5(b,d)] was weaker than that in the core zone [Figure 5(a,c)]. Figure 5(c) indicated that the core layers in the PPR/Ca-Pim samples owned the strongest β diffractions (110_β and 111_β).

The X_c values of PPR samples with and without β-NAs were evaluated by a conventional peak-fitting method. The 1D WAXD profiles of PPR samples with β-NAs were fitted by nine Gaussian plus Lorentz type peaks, that is, two β-crystal peaks, five α-crystal peaks, and two amorphous peaks. The center positions of these peaks were fixed by optimization.[43,44] X_c was calculated according to eq. (1):

$$X_c = \frac{\sum A_{\text{cryst}}}{\sum A_{\text{cryst}} + \sum A_{\text{amor}}} \tag{1}$$

where A_{cryst} and A_{amor} are the areas of the fitted peaks of the crystalline and amorphous phases, respectively. The X_c values of the core layer and skin layer in PPR samples with different β-NA contents are displayed in Figure 6. The X_c of the skin layer was lower than the core layer in both the PPR/TMB-5 and PPR/Ca-Pim systems. This result could be explained by the fast cooling process that the polymer melt experienced during injection molding. The X_c of PPR with TMB-5 was slightly higher than that of PPR/Ca-Pim in both the core and skin layers; therefore, the flexural moduli of the PPR/TMB-5 samples were larger than those of the PPR/Ca-Pim samples at the same β-NA content [shown in Figure 1(b)]. The crystalline region, composed of the ordered packing of polymer chains, exhibited better rigidity than the disordered amorphous region.

k_β

k_β was calculated according to the equation proposed by Turner-Jones *et al.*,[45] which is defined as follows:

$$k_\beta = \frac{A(110_\beta)}{A(110_\beta) + A(110_\alpha) + A(040_\alpha)A(130_\alpha)} \tag{2}$$

where $A(110_\alpha)$, $A(040_\alpha)$, $A(130_\alpha)$, and $A(110_\beta)$ are the corresponding areas of the main reflection peaks of the α and β crystals, respectively.

As shown in Figure 7(a), k_β in PPR/TMB-5 first increased with the β-NA content and then decreased when the content increased further. The k_β reached its maximum at 0.05 and 0.25 wt % in the core and skin layer, respectively. It is known that the shear stress, cooling rate, and nucleating efficiency of β-NA have an impact on the β-crystal fraction in polypropylene samples. Although shear[44] and NA can induce β crystals separately in iPP, the application of shear on β-nucleated iPP was found to be detrimental for the formation of β crystals.[46,47] Fast cooling promoted β-crystal formation in PPR/β-NA samples.[29] In our case, the shear flow field and cooling condition were similar

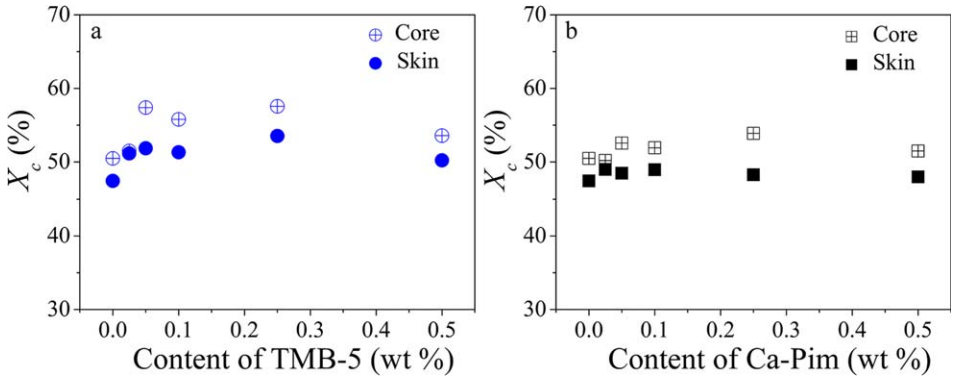

Figure 6. X_c of samples obtained from WAXD data as a function of the β-NA content: (a) PPR/TMB-5 and (b) PPR/Ca-Pim. [Color figure can be viewed in the online issue, which is available at wileyonlinelibrary.com.]

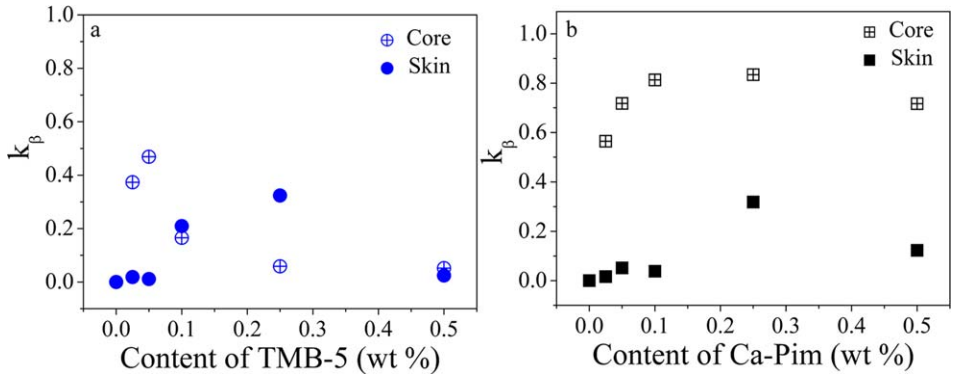

Figure 7. k_β in the PPR samples versus the β-NA content: (a) PPR/TMB-5 and (b) PPR/Ca-Pim. [Color figure can be viewed in the online issue, which is available at wileyonlinelibrary.com.]

during the injection-molding process. TMB-5 was found to be partially or completely dissolved in the iPP melt; this depended on the content and melt temperature.[26,48] According to the temperature/composition diagram of the iPP/TMB-5 mixture reported by Wang *et al.*,[48] only TMB-5 contents below 0.05 wt % could be totally dissolved in the PPR melt at 215°C in our study. The different morphologies of TMB-5 in the PPR/0.05 wt % TMB-5 and PPR/0.25 wt % TMB-5 samples led to the different nucleating efficiencies.k_β in the core layer of PPR/Ca-Pim was always larger than that in the skin layer. k_β in the core and skin layers of PPR/Ca-Pim shared the same variation trend against the Ca-Pim content and reached a maximum at 0.25 wt % [Figure 7(b)]. We noticed that k_β in the skin layer reached its maximum at 0.25 wt % in both the TMB-5 and Ca-Pim systems. k_β in PPR/Ca-Pim was larger compared with PPR/TMB-5; this was due to the difference in the β-nucleation efficiency of these two kinds of β-NAs. TMB-5 has dual nucleating effects[26,35]; that is, it can induce the nucleation of both α and β crystals. Although Ca-Pim is an efficient β-NA that can selectively induce the formation of β crystals, it is worth mentioning that the variation trends of k_β in the core layer of the PPR/β-NAs systems were consistent with the impact strength results shown in Figure 1(a). The quantitative correlation between them are presented later.

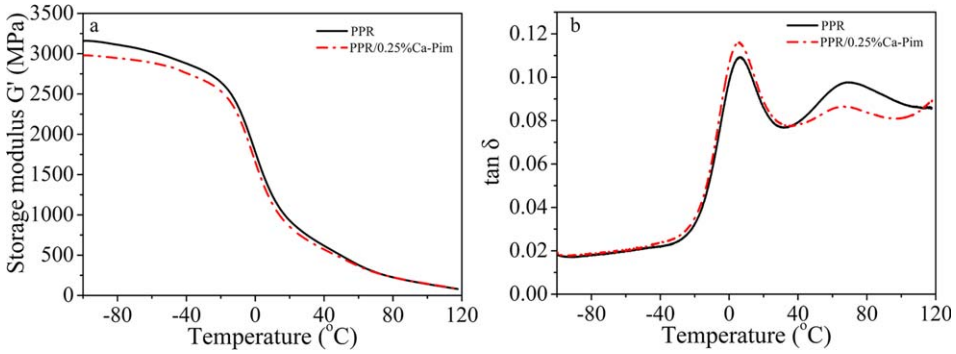

Figure 8. (a) G′ and (b) tan δ as a function of temperature for PPR and PPR containing 0.25 wt % Ca-Pim. The heating rate was 3°C/min. [Color figure can be viewed in the online issue, which is available at wileyonlinelibrary.com.]

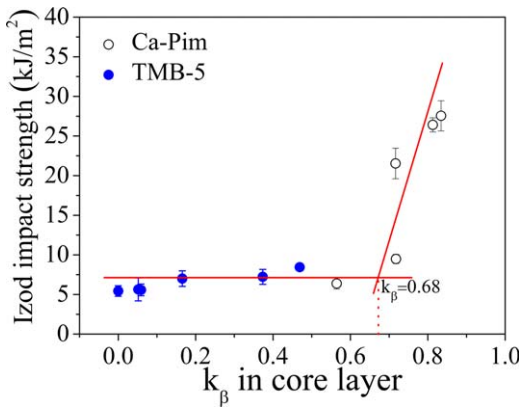

Figure 9. Relationship between the Izod impact strength and k_β in the core layer of PPR. The different k_β values were obtained with different β-NAs, and the transition value was $k_\beta = 0.68$. [Color figure can be viewed in the online issue, which is available at wileyonlinelibrary.com.]

DMA

DMA can provide more information about the microstructures of the samples. Figure 8 gives the storage modulus (G') and mechanical loss factor (tan δ) values for the pure PPR and PPR containing 0.25 wt % Ca-Pim which had the highest β-crystal content (designated as β-PPR). G' of the pure PPR was higher than β-PPR. This was ascribed to the higher rigidity of α crystals compared to β crystals in polypropylene.[14,49] The peak at about 6°C in Figure 8(b) was related to the glass transition of the unrestricted amorphous phase. An increase in the intensity of the glass-transition peak with the β-crystal content was observed. A similar result was reported by Zhang and Shi.[7] The peak around 70°C was the α_c relaxation; this was associated with the relaxation of restricted amorphous copolymer chains in the rigid amorphous region[6,50,51] or helical jumps between the crystallites and the amorphous region.[52] The temperature of the α_c relaxation of β-PPR was lower than that of PPR. This indicated that the mobility of the molecular chains in β-PPR was higher than that in PPR. The excellent toughness of PPR with a high k_β value may have been related to this result.

Relationship between the Mechanical Properties and Structure

A number of factors affect the mechanical properties of the injection-molded polypropylene parts; these factors include the crystallinity, the skin–core ratio, and the orientation.[53,54] The toughness of polypropylene was expected to be improved by the existence of β crystals. However, the direct relationship between the toughness and β-crystal fraction has not been established. In general, the core layer is more ductile than the skin layer,[38,55] so the skin layer provides a minor contribution to the toughness. As shown in Figure 9, the notched Izod impact strength was plotted against k_β in the core layer of PPR. It was interesting to find that there existed a correlation between the impact strength and k_β in the core layer of the specimens. The toughness of PPR/β-NA did not change a lot when k_β was lower than a transition value of about 0.68. However, it increased dramatically when the k_β in the core layer was higher than 0.68. The transition value of k_β was thought to be in line with the brittle–ductile transition in the PPR samples. To directly understand the fracture mode of the PPR samples, the fracture surfaces of PPR samples with different k_β values were observed by SEM, and the results are shown in Figure 10. In the absence of β crystals, the PPR displayed a smooth fracture surface without a plastic deformation zone [Figure 10(a)]. The sample with 0.05 wt % TMB-5 ($k_\beta = 0.47$) exhibited a mixed fracture surface, which contained a part of the plastic deformation zone concentrated in the region near the notch [Figure 10(b)]. As presented in Figure 10(c), the whole fracture surface of PPR with 0.25 wt % Ca-Pim ($k_\beta = 0.83$) was rough; this corresponded to the feature of ductile fracture. The brittle–ductile transition value of k_β may also exist in other β-nucleated polypropylene and polypropylene random copolymer systems. Our results indicate that k_β should exceed a transition value to obtain a polypropylene sample with a high toughness.

CONCLUSIONS

The structure and mechanical properties of PPR samples with two kinds of β-NAs (TMB-5 and Ca-Pim) were studied. Injection-molded specimens displayed a nonuniform structure with a highly oriented skin layer and weakly oriented core layer. The addition of β-NAs to the PPRs was effective for improving the toughness without sacrifices of the tensile and flexural properties. The flexural modulus of PPR was even enhanced by the introduction of TMB-5 because of the increase in crystallinity both in the skin and core layers. The correlation between the toughness and k_β in the core layer was established. A critical

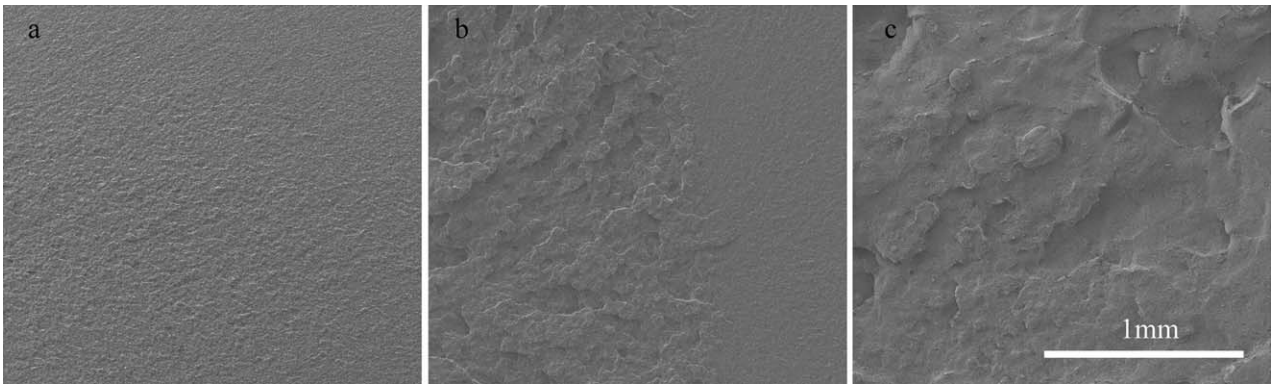

Figure 10. SEM images of the fracture surface of PPR with different k_βs in the core layer: (a) pure PPR with $k_\beta = 0$, (b) PPR/0.05 wt % TMB-5 with $k_\beta = 0.47$, and (c) PPR/0.25 wt % Ca-Pim with $k_\beta = 0.83$. The fracture surface was obtained at room temperature, and the notch was on the left side.

value of k_β of 0.68 was identified for the brittle–ductile transition of PPR.

ACKNOWLEDGMENTS

Financial support from the National Natural Science Foundation of China (contract grant number 51203170) is gratefully acknowledged. G. Liu is grateful for the financial support of the Youth Innovation Promotion Association of the Chinese Academy of Sciences (contract grant number 2015026). The Shanghai Synchrotron Radiation Facility is acknowledged for kindly providing the beam time.

REFERENCES

1. Raab, M.; Kotek, J.; Baldrian, J.; Grellmann, W. *J. Appl. Polym. Sci.* **1998**, *69*, 2255.
2. Liu, G. M.; Zhang, X. Q.; Liu, C. Y.; Chen, H. Y.; Walton, K.; Wang, D. J. *J. Appl. Polym. Sci.* **2011**, *119*, 3591.
3. Liu, G. M.; Zhang, X. Q.; Li, X. H.; Chen, H. Y.; Walton, K.; Wang, D. J. *J. Appl. Polym. Sci.* **2012**, *125*, 666.
4. Yokoyama, Y.; Ricco, T. *Polymer* **1998**, *39*, 3675.
5. Stephens, C. H.; Poon, B. C.; Ansems, P.; Chum, S. P.; Hiltner, A.; Baer, E. *J. Appl. Polym. Sci.* **2006**, *100*, 1651.
6. Luo, F.; Wang, J. W.; Bai, H. W.; Wang, K.; Deng, H.; Zhang, Q.; Chen, F.; Fu, Q.; Na, B. *Mater. Sci. Eng. A* **2011**, *528*, 7052.
7. Zhang, X. D.; Shi, G. Y. *Polymer* **1994**, *35*, 5067.
8. Papageorgiou, D. G.; Bikiaris, D. N.; Chrissafis, K. *Thermochim. Acta* **2012**, *543*, 288.
9. Karger-Kocsis, J.; Varga, J. *J. Appl. Polym. Sci.* **1996**, *62*, 291.
10. Karger-Kocsis, J.; Varga, J.; Ehrenstein, G. W. *J. Appl. Polym. Sci.* **1997**, *64*, 2057.
11. Kotek, J.; Raab, M.; Baldrian, J.; Grellmann, W. *J. Appl. Polym. Sci.* **2002**, *85*, 1174.
12. Geng, C. Z.; Luo, F.; Wang, K.; Deng, H.; Chen, F.; Fu, Q.; Na, B. *Macromolecules* **2009**, *42*, 9325.
13. Li, Y. J.; Wen, X. Y.; Nie, M.; Wang, Q. *J. Appl. Polym. Sci.* **2014**, *131*, 40605.
14. Aboulfaraj, M.; G'Sell, C.; Ulrich, B.; Dahoun, A. *Polymer* **1995**, *36*, 731.
15. Tordjeman, P.; Robert, C.; Marin, G.; Gerard, P. *Eur. Phys. J. E* **2001**, *4*, 459.
16. Chen, H. B.; Karger-Kocsis, J.; Wu, J. S.; Varga, J. *Polymer* **2002**, *43*, 6505.
17. Pawlak, A. *J. Appl. Polym. Sci.* **2012**, *125*, 4177.
18. Cai, Z. W.; Zhang, Y.; Li, J. Q.; Xue, F. F.; Shang, Y. R.; He, X. H.; Feng, J. C.; Wu, Z. H.; Jiang, S. C. *Polymer* **2012**, *53*, 1593.
19. Bao, R. Y.; Ding, Z. T.; Liu, Z. Y.; Yang, W.; Xie, B. H.; Yang, M. B. *Polymer* **2013**, *54*, 1259.
20. Zhang, C. B.; Liu, G. M.; Song, Y.; Zhao, Y.; Wang, D. *J. Polymer* **2014**, *55*, 6915.
21. Menyhárd, A.; Varga, J.; Molnár, G. *J. Therm. Anal. Calorim.* **2006**, *83*, 625.
22. Varga, J. *J. Therm. Anal. Calorim.* **1986**, *31*, 165.
23. Han, L.; Li, X. X.; Li, Y. L.; Huang, T.; Wang, Y.; Wu, J.; Xiang, F. M. *Mater. Sci. Eng. A* **2010**, *527*, 3176.
24. Varga, J. *J. Macromol. Sci. Phys.* **2002**, *41*, 1121.
25. Varga, J.; Menyhárd, A. *Macromolecules* **2007**, *40*, 2422.
26. Dong, M.; Guo, Z. X.; Yu, J.; Su, Z. Q. *J. Polym. Sci. Part B: Polym. Phys.* **2008**, *46*, 1725.
27. Kersch, M.; Pischke, L.; Schmidt, H. W.; Altstädt, V. *Polymer* **2014**, *55*, 3227.
28. Busse, K.; Kressler, J.; Maier, R. D.; Scherble, J. *Macromolecules* **2000**, *33*, 8775.
29. Varga, J.; Schulek-Tóth, E. *J. Therm. Anal.* **1996**, *47*, 941.
30. Obadal, M.; Čermák, R.; Baran, N.; Stoklasa, K.; Šimoník, J. *Int. Polym. Proc.* **2004**, *19*, 35.
31. Bai, H. W.; Wang, Y.; Zhang, Z. J.; Han, L.; Li, Y. L.; Liu, L.; Zhou, Z. W.; Men, Y. F. *Macromolecules* **2009**, *42*, 6647.
32. Shi, Y. H.; Dou, Q. *Polym. Plast. Technol.* **2012**, *51*, 1024.
33. Zhang, C. B.; Liu, G. M.; Jiang, Q. H.; Yang, J.; Zhao, Y.; Wang, D. *J. RSC Adv.* **2015**, *5*, 44610.
34. Guo, L. Y.; Ding, H. L.; Li, D. J.; Zheng, D.; Chen, J.; Qian, Y. Y. *Chin. J. Polym. Sci.* **2015**, *33*, 256.
35. Na, B.; Lv, R. H.; Xu, W. F.; Chen, R.; Zhao, Z. X.; Yi, Y. *Polym. Int.* **2008**, *57*, 1128.
36. Xu, L. L.; Xu, K.; Zhang, X. J.; Liu, F. Y.; Chen, M. C. *Polym. Adv. Technol.* **2010**, *21*, 807.
37. Kantz, M. R.; Newman, H. D.; Stigale, F. H. *J. Appl. Polym. Sci.* **1972**, *16*, 1249.
38. Yu, X. F.; Wu, H.; Li, J.; Guo, S. Y.; Qiu, J. H. *Polym. Eng. Sci.* **2009**, *49*, 703.
39. Stocker, W.; Schumacher, M.; Graff, S.; Wittmann, J. C.; Lotz, B. *Macromolecules* **1998**, *31*, 807.
40. Iijima, R.; Kawai, T.; Yamamoto, Y.; Kimura, T. *Polymer* **2002**, *43*, 7301.
41. Pandini, S.; Baldi, F.; Paderni, K.; Messori, M.; Toselli, M.; Pilati, F.; Gianoncelli, A.; Brisotto, M.; Bontempi, E.; Riccò, T. *Polymer* **2013**, *54*, 4253.
42. Zhang, C. Y.; Wang, B.; Yang, J. J.; Ding, D. W.; Yan, X. R.; Zheng, G. Q.; Dai, K.; Liu, C. T.; Guo, Z. H. *Polymer* **2015**, *60*, 40.
43. Ran, S. F.; Zong, X. H.; Fang, D. F.; Hsiao, B. S.; Chu, B.; Phillips, R. A. *Macromolecules* **2001**, *34*, 2569.
44. Somani, R. H.; Hsiao, B. S.; Nogales, A.; Fruitwala, H.; Srinivas, S.; Tsou, A. H. *Macromolecules* **2001**, *34*, 5902.
45. Jones, A. T.; Aizlewood, J. M.; Beckett, D. R. *Makromol. Chem.* **1964**, *75*, 134.
46. Huo, H.; Jiang, S. C.; An, L. J.; Feng, J. C. *Macromolecules* **2004**, *37*, 2478.
47. Chen, Y. H.; Mao, Y. M.; Li, Z. M.; Hsiao, B. S. *Macromolecules* **2010**, *43*, 6760.

48. Han, R.; Li, Y. J.; Wang, Q.; Nie, M. *RSC Adv.* **2014**, *4*, 65035.
49. Coulon, G.; Castelein, G.; G'Sell, C. *Polymer* **1999**, *40*, 95.
50. Boyd, R. H. *Polymer* **1985**, *26*, 323.
51. Read, B. E. *Polymer* **1989**, *30*, 1439.
52. Hu, W. G.; Schmidt-Rohr, K. *Acta Polym.* **1999**, *50*, 271.
53. Phillips, R.; Herbert, G.; News, J.; Wolkowicz, M. *Polym. Eng. Sci.* **1994**, *34*, 1731.
54. van der Wal, A.; Mulder, J. J.; Gaymans, R. *J. Polymer* **1998**, *39*, 5477.
55. Bowman, J.; Harris, N.; Bevis, M. *J. Mater. Sci.* **1975**, *10*, 63.